Biotechnology Research and Innovation (2017) 1, 112–122

Biotechnology Research & Innovation

http://www.journals.elsevier.com/biotechnology-research-and-innovation/

RESEARCH PAPER

Pharmacophore modeling and 3D QSAR studies for prediction of matrix metalloproteinases inhibitory activity of hydroxamate derivatives

Dharmender Rathee[a], **Viney Lather**[b], **Harish Dureja**[a,*]

[a] *Department of Pharmaceutical Sciences, Maharshi Dayanand University, Rohtak, Haryana, India*
[b] *Department of Pharmaceutical Chemistry, JCDM College of Pharmacy, Sirsa, Haryana, India*

Received 3 August 2017; accepted 4 October 2017
Available online 25 October 2017

KEYWORDS
Pharmacophore modeling;
3D-QSAR;
MMP-2;
MMP-9;
MMP inhibitors;
Hydroxamate derivatives

Abstract In order to develop potent inhibitors of matrix metalloproteinase (MMP-2 and MMP-9) as anticancer agents, pharmacophore modeling and three-dimensional quantitative structure–activity relationship (3D-QSAR) models were established using PHASE 3.0. A pharmacophore 5-point (AAARR) model was developed for the studied dataset and the generated model was used to derive the predictive atom-based 3D-QSAR models. After identifying a valid hypothesis, we developed 3D-QSAR models applying the PLS algorithm. The selected 3D-QSAR models were suggestive of the vitality of the electron-withdrawing feature for the MMPs inhibitory potential. In addition, hydrophobic groups, hydrogen bond donor groups, positive ionic and negative ionic features also positively contributed to the MMPs inhibitory potential along with the electron-withdrawing feature. The developed models were statistically robust (MMP-2 $Q^2 = 0.51$; pred $R^2 = 0.67$; MMP-9 $Q^2 = 0.59$; pred $R^2 = 0.77$). The QSAR results help in identifying a relationship between structural features of hydroxamate derivatives and their activities which could be useful to design newer MMP inhibitors.

Introduction

Cancer cells possess a broad spectrum of migration and invasion mechanisms and metastasis is one of the major causes for mortality in cancer patients. Highly malignant cancers have metastasis as an important characteristic with poor clinical outcome. Malignant tumor progression mainly depends upon the capacity to invade, metastasize, and to promote the angiogenic host response. Metastasis cancer cells have acquired one critical characteristic; that is the ability to dissolve the extracellular matrix (ECM) and basement membranes (Rathee, Thanki, Bhuva, Anandjiwala, & Agrawal, 2013). The growth of a tumor and its ability to metastasize mainly depends on angiogenesis (Folkman, 1971). In addition, angiogenesis is critically important for embryo and female reproductive cycles vascular remodeling and also for wound healing specifically in the adults.

* Corresponding author.
E-mail: harishdureja@gmail.com (H. Dureja).

https://doi.org/10.1016/j.biori.2017.10.002

However, aberrant angiogenesis occurs in certain pathological conditions, like diabetic retinopathy, psoriasis, cancer, hemangiomas, and rheumatoid arthritis (Liekens, Clercq, & Neyts, 2001). Since, endothelial cells invasion/migration into surrounding tissues/stroma involves in angiogenesis, proteases like matrix metalloproteinases (MMPs) are vitally significant.

MMPs belongs to a family of zinc-dependent, calcium-containing endoproteinases which are involved in degradation of ECM components and tissue remodeling at the physiological pH values, mainly in cell motility and angiogenesis (Kontogiorgis, Papaioannou, & Hadjipavlou-Litina, 2005). MMPs are involved in various processes such as ovulation, implantation of the blastocyst, development of embryo, morphogenesis, nerve growth, tissue remodeling and resorption (in wound healing case), bone remodeling, arthritis (both osteoarthritis and rheumatoid arthritis), gastric ulceration, corneal and skin ulcer, multiple sclerosis, angiogenesis, apoptosis, cancer invasion and metastasis, pulmonary emphysema, rupture of atherosclerotic plaque, aortic aneurysms, congestive heart failure, breakdown of blood-brain barrier, Crohn's disease, periodontal disease, psoriasis, dermatitis and Alzheimer's disease (Scozzafava & Supuran, 2000). Virtually, all human cancers generally abundantly express MMPs. MMPs expression from tumor stromal cells passing through paracrine secretion of growth factors and cytokines is induced by cancer cells (Egeblad & Werb, 2002). High levels of expression of certain MMPs, either by the infiltrating inflammatory cells, by the tumor cells themselves or by stromal fibroblasts, are correlated with poor prognosis and metastatic potential and/or tumor invasion (Vihinen & Kähäri, 2002). Several mechanisms are involved for the role of MMPs in the cancer progression. At first, it was taken into consideration that the MMPs mediate metastasis and invasion chiefly by matrix remodeling thus allowing tumor cells access to lymphatic and blood vessels. The fact for this mechanism is mainly based on the increased cell lines invasiveness, which further over expresses the MMPs. In recent times, it is evident that MMPs can play a role in primary tumor growth and it involves the release of MMP-mediated tumor angiogenesis or stroma-bound growth factors (Summers & Davidsen, 1998).

Recently, it turn out to be crystal clear about the more complex role of MMPs in angiogenesis rather than simply degrading the ECM in order to facilitate the invading endothelial cells (Liekens et al., 2001; Stetler-Stevenson, 1999). Also, it is evident about the multiplicity and complexity of the signals that commence and sustain angiogenesis. Growth factors and proangiogenic cytokines include fibroblast growth factors (FGFs), angiopoietins, vascular endothelial growth factors (VEGFs), transforming growth factor-β (TGF-β), tumor necrosis factor-α (TNF-α), platelet-derived growth factors (PDGFs), interleukin-8 (IL-8), epidermal growth factor (EGF), and angiogenin which are secreted by pericytes, keratinocytes (during epidermal wound healing), inflammatory cells (such as macrophages and mast cells), or tumor cells. Some of these growth factors and proangiogenic cytokines act by binding directly to their respective receptors present on endothelial cells to induce migration and/or proliferation, whereas in order to stimulate angiogenesis others act on inflammatory cells or local stromal cells (Li, Zhang, & Kirsner, 2003; Weinstat-Saslow & Steeg, 1994). For the ''angiogenic switch'' in cancer angiogenesis, MMP-2 and MMP-9 (gelatinases) have been shown to be significant when cancers (or preneoplastic lesions) become vascularized for the first time. In angiogenic islets, MMP-2 and MMP-9 expression was up-regulated in comparison with preangiogenic islets, however, it was determined that MMP-2 expression contributed to cancer growth (using MMP knockout mice), while MMP-9 expression was important for angiogenic switch (Yu & Stamenkovic, 2000). Invasion and metastasis capability, and/or risk of recurrence have been correlated in particular with tumor expression of MT1-MMP and various other MMPs (such as MMP-1, -2, -3, - 7, -9, -13) (Vihinen & Kähäri, 2002).

The MMPs inhibition has been the subject of intense research interest in the pharmaceutical industry in recent years (Johnson, Dyer, & Hupe, 1998; Morphy, Millican, & Porter, 1995; Zask, Levin, Killar, & Skotnicki, 1996). Various available synthetic MMP inhibitors are classified as tetracycline analogues, hydroxamates, carboxylates, barbiturates, thiols, phosphonates, etc. (Subramaniam, Malik, & Srivastava, 2009). The design of new MMPs inhibitors provides an opportunity to develop new drug candidates, as in several pathological states aberrant MMPs activities are involved (Mori et al., 2013). The design of various MMPs inhibitors for use as therapeutic agents has been an exceptionally active area of research, specifically in the treatment of arthritis and cancer (Skiles, Gonnella, & Jeng, 2001; Zask et al., 1996).

For the speedy discovery and development of novel anticancer therapeutic agents, the technological advancement and broader application of experimental methods grasp vast assurance as foundations. To achieve this target, computer-aided drug discovery (CADD) has become progressively more important, due to certain advantages such as much less investment in technology, time is required and resources (Wilson & Muftuoglu, 2012). Various cases of structure-based drug design's successful applications have been reported in the recent years (Combs, 2007; Coumar et al., 2009; Khan et al., 2010; van Montfort & Workman, 2009). With the help of computational methods, the chemical compounds with potentially higher affinity for the target can be rationally designed by utilizing the given three dimensional structure of a target molecule. Based on this pharmacophore model (binding site-derived), the results consist of a compilation of virtual ligands complementary to a three dimensional structure of the binding pocket- a pattern of putative interaction sites (Wilson & Muftuoglu, 2012). During the identification of p53 upregulated modulator of apoptosis (PUMA) inhibitors structure-based pharmacophore modeling was successfully used (Mustata et al., 2011).

Several QSAR studies have been published for hydroxamate derivatives (Gupta, 2015; Stephen, Nicolas, Cécile, & Martin, 2001). Previously reported studies discussed various QSAR (Nirmala, Adimulam, & Seetharamaiah, 2016, chap. 4; Roy, Pal, De, & Sengupta, 2001; Zheng, Wen, & Guillaume, 2008) approaches against MMPs (MMP-1, MMP-2, MMP-8, MMP-9, MMP-13), however, 3D-QSAR (three-dimensional quantitative structure–activity relationship) approach was not discussed. Nermala et al. employed multiple regression procedure to perform QSAR analysis on a set of 72 α-sulfone hydroxamate MMP-13 inhibitors. Roy et al. performed QSAR analyses on N-[(substituted

phenyl)sulfonyl]-N-4-nitrobenzylglycine hydroxamates MMP inhibitors, using linear free energy related (LFER) model. Jianbin et al. derived QSAR models using comparative molecular field analysis (CoMFA), comparative molecular similarity indices analysis (CoMSIA) and molecule docking on a set of galardin derivatives (hydroxamic acid).

In the current research work, pharmacophore models (MMP-2 and MMP-9) were developed in order to predict the MMPs inhibitory potential of hydroxamate derivatives. Based on 3D-QSAR approach two different predictive models have been developed by using PHASE module of Schrödinger suite. ''The 3D-QSAR approach involves the development of a common pharmacophore hypothesis which is built on the principle of identification and alignment of pharmacophoric features of the chemical structures''. Using the structures of training set molecules which match the pharmacophore on three or more sites, 3D-QSAR models were developed for the pharmacophore hypothesis by using Partial Least Square (PLS) method for statistical analysis. The developed pharmacophore hypothesis and generated volume occluded maps assist in analyzing the observed activity variation by the structural features variation.

Materials and methods

Software and hardware

The pharmacophore modeling and 3D-QSAR studies were carried out using PHASE v.3.0 module incorporated in the Maestro 8.5 molecular modeling package from Schrodinger, LLC, New York USA, installed on Windows 7 operating system with Intel Pentium IV, Core 2 Duo processor (Phase, 2008).

Dataset used for experimental analysis

The dataset used for the experimental work comprises of a series of 33 hydroxamate derivatives as MMP inhibitors (Scozzafava & Supuran, 2000). Of these 33 derivatives, we selected 30 molecules for the MMP-2 model and 32 molecules for the MMP-9 model. The in vitro pharmacological activity data was presented as IC_{50} values and these IC_{50} values were then converted to pIC_{50} by using the formula ($pIC_{50} = -\log IC_{50}$). The experimental dataset consisted of a diverse range of molecules with highly active, inactive and moderately active molecules. Fig. 1 shows the common structure of the hydroxamate derivatives employed for the study. Further, Tables 1 and 2 depict the pIC_{50} values for all of the compounds used in the current study.

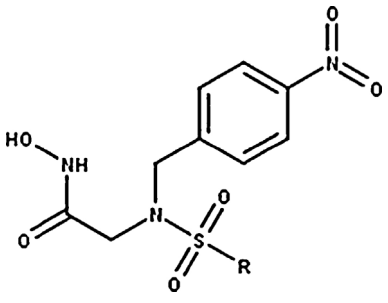

Figure 1 Common structure of hydroxamate derivatives.

30 molecules were totally used for MMP-2 inhibitory activity model development, and of these, 25 compounds were randomly chosen for training set and 5 molecules were selected for test set, whereas for the model development of MMP-9 inhibitory activity 32 molecules were used in total, and of these 25 molecules were randomly chosen for training set and 7 molecules were selected to be a part for test set.

Phase methodology

The step wise methodology used in the current study for the generation of pharmacophore model followed by development of QSAR model had already been discussed in the previous publication by Lather et al. (2008).

> ''*PHASE is a versatile product for pharmacophore perception, structural alignment, activity prediction, and 3D database creation and searching. Given a set of molecules with an affinity for a particular target, PHASE utilizes fine-grained conformational sampling and a range of scoring techniques to identify a common pharmacophore hypothesis, which conveys characteristics of the 3D chemical structures that are reported to be critical for binding. Each hypothesis is accompanied by a set of aligned conformations that suggest the relative manner in which the molecules are likely to bind to the receptor*'' (Lather et al., 2008).

Ligand preparation

The LigPrep software (MMFF force field) implemented within PHASE was used for the 3-D conversion and minimization.

The pharmacophore model development requires all-atom 3-D structures that are pragmatic presentations of the molecular structure used in the experiment. Based on the fact that most of the ligands are flexible it is really imperative that a range of thermally accessible conformational states were considered, so that the probability of finding somewhat close to the putative binding mode should increase. In development of pharmacophore model, 2 built-in approaches are typically provided by PHASE module, and in both the approaches the MacroModel conformational search engine was employed (Dixon et al., 2006).

A rapid torsion angle search approach was used to generate the conformers, followed by each generated structure minimization by using LigPrep MMFF force field, with implicit distance dependent dielectric solvent model. By using a pre-process minimization of 100 steps and 50 steps for post-process minimization, a maximum of 100 conformers per structure were generated. A minimum atom deviation of 2.00 Q and relative energy window of 11.4 kcal/mol (50 kJ/mol) was used to filter each minimized conformer (Lather et al., 2008).

Pharmacophore model development

In order to create sites for all the ligands, a pharmacophore model generation used a defined set of pharmacophoric features. In order to facilitate non-covalent binding between the ligand and its target receptor, each ligand structure coincides with various chemical features. In 3-D space, it is presented by a set of points. PHASE module provides an in built set of six pharmacophore features i.e. hydrophobic group (H), hydrogen bond donor (D), hydrogen bond

Table 1 Experimental dataset employed for 3D-QSAR study along with predicted and actual pIC_{50} values against MMP-2.

Compound	QSAR set	R	Actual pIC_{50}	Predicted pIC_{50}	Residuals
B1	Training	—CH_3	7.72	7.66	−0.05
B2	Test	—CF_3	7.83	7.97	0.14
B3	Training	—CCl_3	7.77	7.82	0.05
B4	Training	—*n*-C_4F_9	8.82	8.89	0.07
B7	Training	—C_6H_5	7.75	8.06	0.31
B8	Training	—CH_2Ph	7.75	7.47	0.27
B9	Training	4-F-C_6H_4	7.82	8.03	0.21
B10	Training	4-Cl-C_6H_4	7.82	7.91	0.09
B11	Test	4-Br-C_6H_4	7.89	7.69	−0.19
B12	Test	4-I-C_6H_4	7.72	7.80	0.08
B13	Training	4-CH_3-C_6H_4	7.7	7.80	0.10
B14	Training	4-O_2N-C_6H_4	8.05	7.79	−0.25
B15	Training	3-O_2N-C_6H_4	7.92	7.66	−0.25
B16	Training	2-O_2N-C_6H_4	7.82	7.69	−0.12
B17	Training	3-Cl-4-O_2N-C_6H_3	8.16	8.25	0.09
B18	Test	4-AcNH-C_6H_4	8.1	7.69	−0.40
B19	Training	4-BocNH-C_6H_4	8	7.97	−0.02
B20	Training	3-BocNH-C_6H_4	7.96	8.28	0.32
B21	Training	—C_6F_5	9.16	8.59	−0.56
B22	Training	3-CF_3-C_6H_4	8.96	8.56	−0.39
B23	Training	2,5-$Cl_2C_6H_3$	8	7.93	−0.06
B24	Training	4-MeO-C_6H_4	7.75	7.61	−0.13
B25	Test	2,4,6-$Me_3C_6H_2$	7.6	7.72	0.12
B26	Training	4-MeO-3-BocNH-C_6H_3	8.3	8.07	−0.22
B27	Training	2-HO-3,5-Cl_2-C_6H_2	7.92	8.28	0.36
B28	Test	3-HOOC-C_6H_4	8.52	8.37	−0.14
B30	Training	1-Naphthyl	7.41	7.77	0.36
B31	Training	2-Naphthyl	7.48	7.85	0.37
B32	Training	2-Thienyl	7.39	7.33	−0.05
B33	Training	5-Me_2N-1-naphthyl	7.89	7.94	0.05

3D-QSAR, 3-dimensional quantitative structure activity relationship; pIC_{50}, inhibitory concentration 50; MMP-2, matrix metalloproteinase-2.

acceptor (A), aromatic ring (R), positively ionizable (P) and negatively ionizable (N). Some rules are applied for mapping the positions of pharmacophore sites and these are known as feature definitions. Further, these are internally represented by a defined set of SMARTS patterns (Dixon et al., 2006). In addition, each pharmacophore feature is defined by a set of chemical structure patterns. During pharmacophore sites creation a default setting having H, D, A, P, N, and R was used and in the present study user-defined feature was not employed.

The pharmacophore amongst all conformations of the ligand in the active site was examined, and the pharmacophores were grouped together based on identical set of features with very similar spatial arrangements. A tree-based partitioning technique was used to identify common pharmacophores that groups similar pharmacophores as per their inter-site distances (i.e., the site to site distances in the pharmacophore). After, application of default feature definitions to each ligand, the common pharmacophores containing five or more sites using a terminal box size of 1 Å were generated, where all of the active molecules should match. For alignment of the actives to the hypotheses and calculation of the score for the actives a score hypotheses step was employed. A hypothesis was provided by the developed pharmacophore which explained the binding of the active molecules to their receptors. This scoring procedure provides the positioning for the different hypotheses, and helps to make rational choices about the hypotheses which are mostly suitable for further investigations. Common pharmacophores with statistically significant values were chosen for molecular alignments.

3D-QSAR

PHASE module provides the basis of building the 3D QSAR models by using the ligands activities that matches a reported hypothesis. ''*PHASE 3D-QSAR models are based on PLS regression, which applied to a large set of binary valued variables. In the QSAR model the independent variables are derived from a regular grid of cubic volume elements that span the space occupied by the training set ligands. Each ligand is represented by a set of bit values (0 or 1) that indicate which volume elements are occupied by a Van der Waals surface model of the ligand*''.

In order to distinguish between different types of atoms which occupy the same region of space, in the grid a given cube might be allocated as many as six bits, which accounts for 6 different atoms classes. The following are the six atoms classes:

Table 2 Experimental dataset employed for 3D-QSAR study along with predicted and actual pIC_{50} values against MMP-9.

Compound	QSAR set	R	Actual pIC_{50}	Predicted pIC_{50}	Residuals
B1	Test	CH_3	7.52	7.55	0.03
B2	Training	CF_3	7.54	7.69	0.15
B3	Training	CCl_3	7.6	7.64	0.04
B4	Training	*n*-C_4F_9	8.7	8.57	−0.12
B5	Training	*n*-C_8F_{17}	8.89	8.97	0.08
B6	Training	Me_2N	7.37	7.28	−0.08
B7	Training	C_6H_5	7.82	7.96	0.14
B8	Training	$PhCH_2$	7.8	7.34	−0.45
B9	Test	4-F-C_6H_4	7.85	8.05	0.20
B10	Training	4-Cl-C_6H_4	7.77	7.95	0.18
B11	Test	4-Br-C_6H_4	7.68	7.64	−0.03
B12	Test	4-I-C_6H_4	7.8	7.63	−0.16
B13	Training	4-CH_3-C_6H_4	7.57	7.63	0.06
B14	Training	4-O_2N-C_6H_4	8.1	7.83	−0.26
B15	Test	3-O_2N-C_6H_4	8.1	8.23	0.13
B16	Test	2-O_2N-C_6H_4	7.85	7.98	0.13
B17	Training	3-Cl-4-O_2N-C_6H_3	8.16	8.13	−0.02
B18	Training	4-AcNH-C_6H_4	7.92	7.74	−0.17
B19	Training	4-BocNH-C_6H_4	8	8.02	0.02
B20	Training	3-BocNH-C_6H_4	7.85	8.16	0.31
B21	Training	C_6F_5	9.22	8.50	−0.71
B23	Training	2,5-$Cl_2C_6H_3$	7.77	7.83	0.06
B24	Training	4-MeO-C_6H_4	7.51	7.44	−0.06
B25	Training	2,4,6-$Me_3C_6H_2$	7.41	7.45	0.04
B26	Training	4-MeO-3-BocNH-C_6H_3	8.16	7.87	−0.28
B27	Training	2-HO-3,5-Cl_2-C_6H_2	7.8	8.03	0.23
B28	Training	3-HOOC-C_6H_4	8.6	8.72	0.12
B29	Training	4-HOOC-C_6H_4	8.55	8.58	0.03
B30	Training	1-Naphthyl	7.36	7.72	0.36
B31	Training	2-Naphthyl	7.3	7.52	0.22
B32	Test	2-Thienyl	7.28	7.52	0.24
B33	Training	5-Me_2N-1-naphthyl	8	8.07	0.07

3D-QSAR, 3-dimensional quantitative structure activity relationship; pIC_{50}, inhibitory concentration 50; MMP-9, matrix metalloproteinase-9.

(a) Hydrogen-bond donor (D)
(b) Hydrophobic or non-polar (H)
(c) Negative ionic (N)
(d) Positive ionic (P)
(e) Hydrogen-bond acceptors or electron-withdrawing (A)
(f) Other types (miscellaneous) (O)

PHASE generated 3D-QSAR models are either based on pharmacophore or on atoms, the only difference is either all atoms are considered, or only the pharmacophore sites which can be synchronized en route for the hypothesis. The selection of the type of model to develop mainly depends upon the fact that the training set molecules are congeneric and adequately rigid or not. The atom-based model can work well if the structures have some common structural framework and also contain a comparatively less number of rotatable bonds (Katritzky, Mu, Lobanov, & Karelson, 1996).

Based on the criteria defined above, atom-based 3D-QSAR models were generated for MMP-2 and MMP-9 inhibitory activities using the best 5 point AAARR hypothesis. The hypothesis was generated using 25 molecule training set (for both models) and a grid spacing of 1.0 Q. 3D-QSAR models with three PLS factors were generated and further, validated with predicting activities of molecules in the test set.

Results and discussion

Pharmacophore hypothesis generation

Ligand-based drug design is based on the understanding of known molecules which possessed biological activity to bind to the target of concern. In order to bind to the target a molecule must possess the minimum necessary structural characteristics and these molecules can be used to develop a pharmacophore (Guner, 2000). The hydroxamate derivatives tested as inhibitors for MMP-2 and MMP-9 by Scozzafava and Supuran (2000) were used in the current study to derive a pharmacophore model and to identify the necessary chemical features for the inhibitory effect.

Ligand based approaches consider two or three dimensional shape, chemistry, and pharmacophoric points to assess similarity. For identification of the common pharmacophore hypothesis, the experimental dataset was further

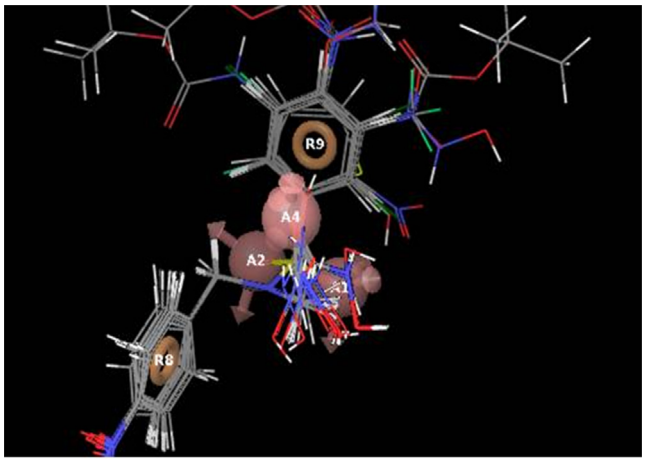

Figure 2 Pharmacophore model (AAARR) generated by PHASE. It illustrates hydrogen bond acceptors (A_1, A_2, A_4; pink color), and aromatic rings (R_8, R_9; brown color) features. All ligands overlapped on the generated model AAARR.

divided into active and inactive sets. Selected features (pharmacophoric) for creating sites were A, H, R, N, and D. Pharmacophore models containing three to six features were generated for this study. For all the molecules in the dataset the identification and creation of pharmacophoric sites was done, followed by generation of common pharmacophore model with AAARR hypothesis. Further, this was subjected to stringent scoring function analysis. The common pharmacophore hypothesis was chosen based on a variant with a site score 0.91, vector score 0.991, and volume score 0.842. The best model comprises of three hydrogen bond acceptors (A) and two aromatic rings (R) and was associated with the five point hypotheses. The hydrogen bond acceptors and aromatic rings were denoted as A_1, A_2, A_3, R_1, and R_2. Fig. 2 represents the pharmacophore hypothesis (AAARR) with all active molecules aligned to it. Further, the AAARR hypothesis matched with all the molecules in the active set. For the generation of MMP-2 and MMP-9 QSAR models the AAARR pharmacophore hypothesis was used.

3D-QSAR studies (MMP-2 and MMP-9 models)

The 3D-QSAR studies for the hydroxamate derivatives were carried out using PHASE module of Schrodinger molecular modeling package to understand the effect of spatial arrangement of structural features on MMP inhibition. In the 3D-QSAR models generation, moderately active or inactive (non modeled) molecules in the experimental dataset were aligned on the common pharmacophore hypothesis based on a match with at least three of the pharmacophoric features. For MMP-2 model, the experimental dataset was divided randomly into a training set of 25 compounds and the test set comprises of 5 compounds whereas, for MMP-9 model, the dataset was divided into a training set comprises of 25 compounds and test set consists of 7 compounds. For a QSAR study, the structural diversity in both the training and test set was given a bias, in order to form the standard 1:5 test set to training set ratio.

Tables 3A and 3B summarize the detailed statistics of the resulting 3D-QSAR models (MMP-2 and MMP-9) based on

Table 3A PHASE 3D-QSAR statistical parameters for MMP-2.

MMP-2 statistical parameters							
R^2	S.D.	*F* value	RMSE	Q^2	Stability	Pearson *R*	*P*
0.67	0.2	23.9	0.21	0.51	0.23	0.75	3.89e−05

3D-QSAR, 3-dimensional quantitative structure activity relationship; MMP-2, matrix metalloproteinase-2; S.D., standard deviation; RMSE, root-mean-square error.

Table 3B PHASE 3D-QSAR statistical parameters for MMP-9.

MMP-9 statistical parameters							
R^2	S.D.	*F* value	RMSE	Q^2	Stability	Pearson *R*	*P*
0.77	0.2	33.6	0.16	0.59	0.30	0.86	6.29e−07

3D-QSAR, 3-dimensional quantitative structure activity relationship; MMP-9, matrix metalloproteinase-9; S.D., standard deviation; RMSE, root-mean-square error.

random test set selection method. Selection of best PLS model is based on an employed statistical analysis which included the R^2 versus RMSE/SD plot. A minima is observed in the RMSE/SD value and a best model was chosen to be PLS factor model. For a reliable model, the squared predictive correlation coefficient should exceed 0.60 (Dureja, Kumar, Gupta, & Madan, 2007; Wold, 1991). In the selection of best model, criteria such as SD and RMSE were also taken into consideration. The statistically significant regression model was supported by the values of F (23.9 and 33.6 for MMP-2 and MMP-9, respectively), and small values of P (variance ratio), which is an indication of a high degree of confidence. Further, the small values of standard deviation of regression (0.2 for both models) and RMSE (0.21 and 0.16 for MMP-2 and MMP-9, respectively) make an apparent inference that the data used for models generation were best for the QSAR analysis. A 3-PLS factor generated 3D-QSAR models with $R^2 = 0.67$ for MMP-2 and 0.77 for MMP-9 (random set selection), indicated a good correlation for the pharmacological activity. Figs. 3(A and B) and 4(A and B) depict the linear plots of actual versus predicted activity for the training and test sets. The validity of each of the models was predicted from the calculated correlation coefficient for the randomly chosen test set comprising of diverse structures. The squared correlation for the test set (random selection ($Q^2 = 0.51$ for MMP-2 and 0.59 for MMP-9)) also signifies the good predictability of the final QSAR models for the test set. The Q^2 was more reliable and robust statistical parameter in comparison to R^2 as it was obtained by external validation method by randomly dividing the dataset into training and test set.

Analysis of atom-based PHASE 3D-QSAR models

The contribution of the substituents to the biological activity whether positively or negatively could be predicted by the visualization of 3D characteristics of the all atom based

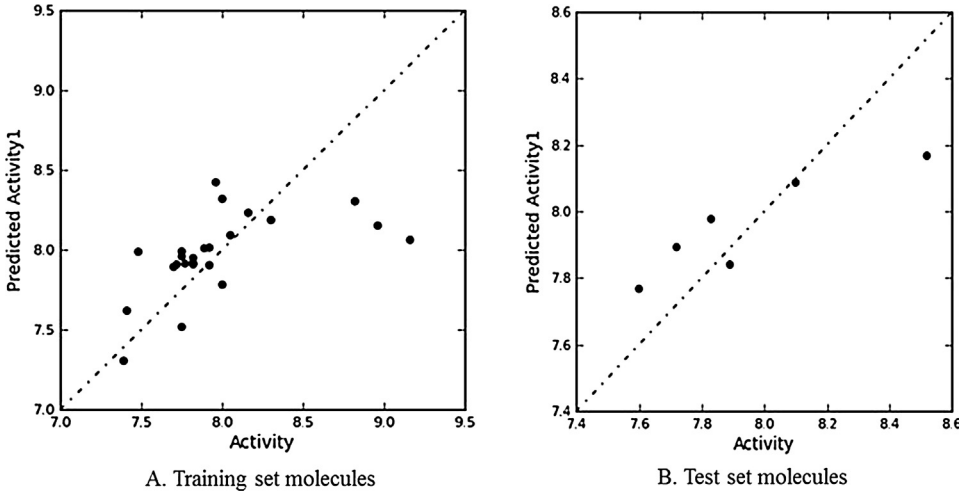

Figure 3 (A and B) Graphical presentation of Actual versus Predicted pIC_{50} of training and test set molecules for MMP-2 model.

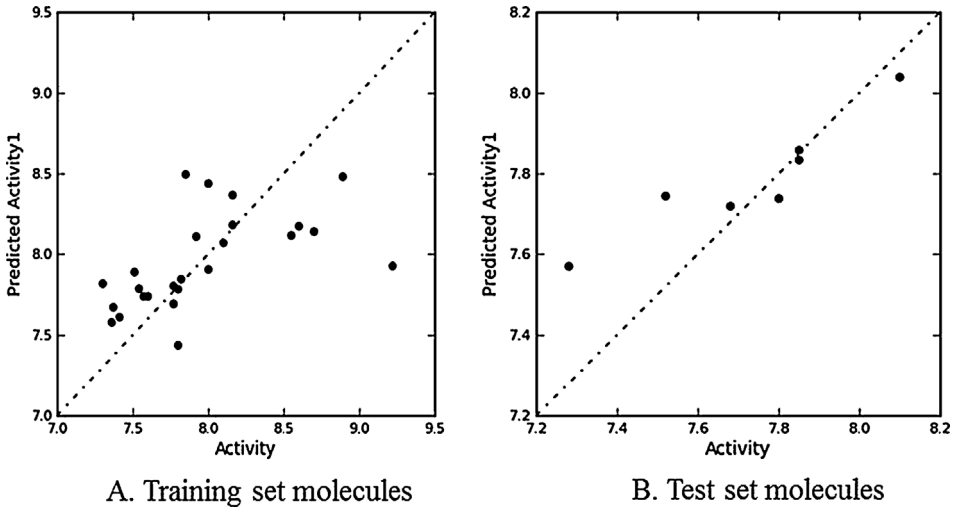

Figure 4 (A and B) Graphical presentation of Actual versus Predicted pIC_{50} of training and test set molecules for MMP-9 model.

QSAR model. Figs. 5 and 6 depict 3D characteristics of the PHASE QSAR models and as the cubes represent the models and color codes as their coefficient values according to the sign. By default the blue color was for positive coefficients and red color was for negative coefficients. Further, an increase in biological activity was indicated by positive coefficients whereas a decrease in biological activity was indicated by the negative coefficients. In order to identify the characteristics of ligand structures whether to facilitate the increase or to decrease the activity the visualization of the coefficients was helpful. This might provides evidence to which functional groups were advantageous or non-advantageous at certain specific positions in a molecule. In 3D plots of the 3D pharmacophore regions the blue color cubes refer to ligand regions in which the specific attribute was important for enhanced biological activity, whereas the red cubes demonstrates that particular functional group or structural feature was not necessary for the biological activity or possibly the reason for decreased binding potency.

MMP-2 model

The volume occlusion maps shown in Fig. 5 for MMP-2 atom based PHASE 3D-QSAR model (electronegative, negative ionic, hydrophobic, positive ionic and other) are represented by color codes. The occlusion maps symbolize the regions of favorable and unfavorable interactions.

Fig. 5A shows the volume occlusion maps of electron-withdrawing groups which indicate the suitable position of electron-withdrawing groups in the phenyl ring attached to the N-2 of the hydroxamate moiety. These analyses points toward the improvements in the MMP-2 inhibitor binding affinity which can be achieved by substituting electron-withdrawing groups on the phenyl ring of hydroxamate moieties at C4 and C5 positions. This was pointing toward the positive potential of electron withdrawing attribute of the molecules and was essential for the MMP-2 activity at this particular position. However, positions C2, C3 and C6 were not favorable for the electron withdrawing groups and probably contribute to decrease in the MMP-2 activity.

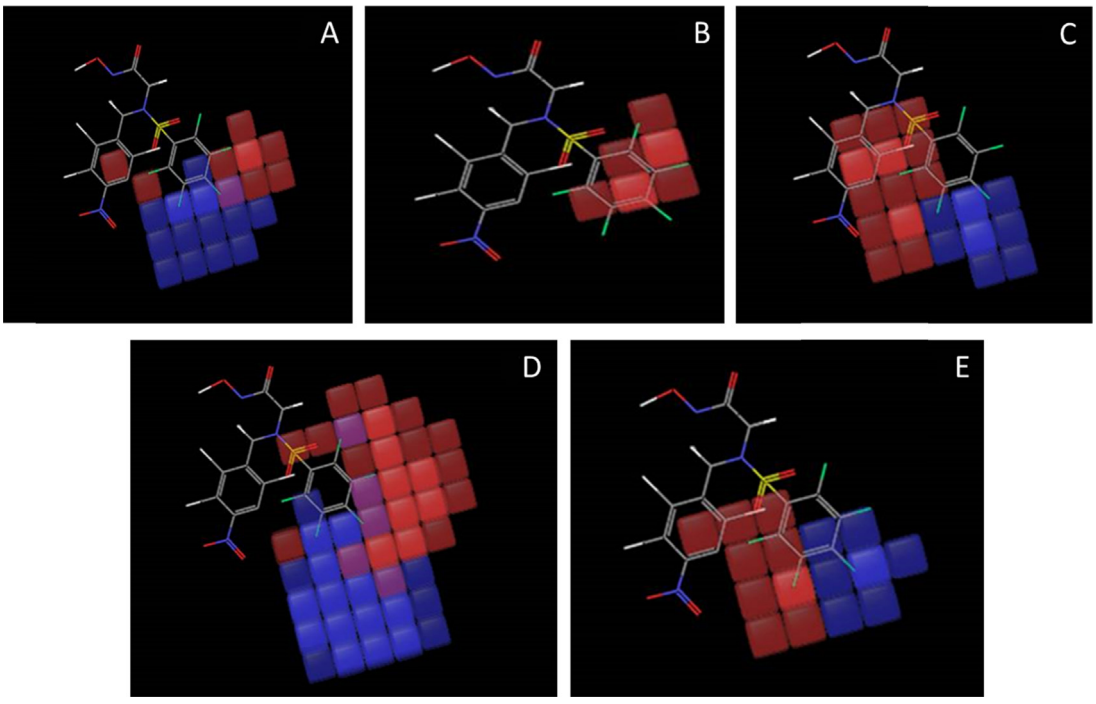

Figure 5 (A–E) Visual representation of atom-based PHASE 3D-QSAR MMP-2 model. (A) Electron withdrawing, (B) other, (C) positive ionic, (D) hydrophobic, and (E) negative ionic. Blue color cubes indicate positive coefficient or increase in activity and red color cubes indicate negative coefficient or decrease in activity.

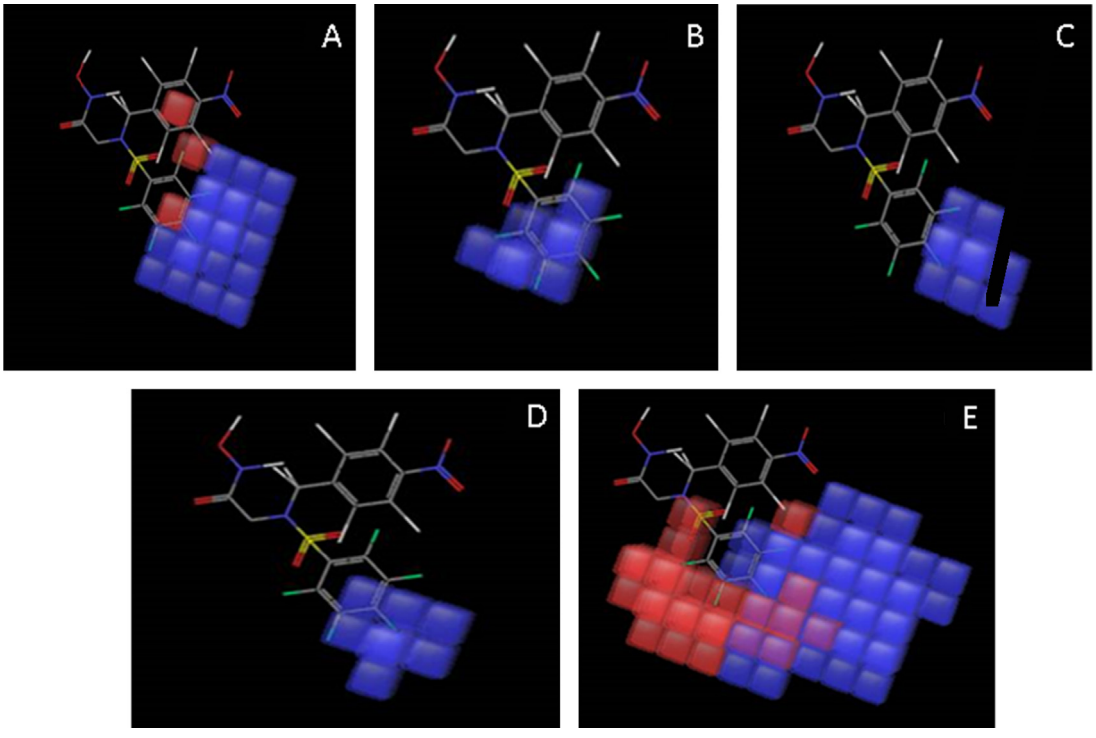

Figure 6 (A–E) Visual representation of atom-based PHASE 3D-QSAR for MMP-9 model. (A) Electron withdrawing, (B) other, (C) negative ionic, (D) positive ionic, and (E) hydrophobic. Blue color cubes indicate positive coefficient or increase in activity and orange color cubes indicate negative coefficient or decrease in activity.

Fig. 5B illustrates the volume occlusion map for other feature and it disfavors the MMP-2 inhibitory activity due to presence of only the red color region.

Fig. 5C shows the volume occlusion map of negative ionic feature which describes the spatial arrangement of favorable ionic interactions to the acceptor groups at the C4 and C5 positions of the phenyl ring. The occlusion map analysis surrounding the active molecules depicts that the blue color cubes observed opposite to the phenyl ring explain a favorable ionic group to an acceptor group available in the protein.

Hydrophobic volume occlusion maps (Fig. 5D) showed blue colored cubes on C4/5 or C5/6 positions of phenyl ring demonstrating that an increase in the hydrophobic character in this region probably improves the activity of the hydroxamate type molecules. The red colored cubes on C2/3 or C3/4 positions were not favoring the assignment of hydrophobic groups.

The volume occlusion maps of positive ionic feature (Fig. 5E) illustrate the spatial arrangement of favorable ionic interactions to donor groups at C3, C4 positions of the phenyl ring. The occlusion map analysis of the phenyl ring of hydroxamate moiety depicts that blue cubes which was observed at the meta, para and meta positions of the phenyl ring describe a favorable ionic group to a donor group in the protein.

Overall, the all atom QSAR model generated by PHASE depicts that substitution at C4 and C5 by different groups like electron-withdrawing, ionic and/or hydrophobic groups play a vital role in the MMP-2 inhibitory activity. The substitutions at other positions i.e. C2, C3 and C6 were not having any significant contribution in the biological activity.

MMP-9 model

The volume occlusion maps shown in Fig. 6 for MMP-9 atom based PHASE 3D-QSAR model (electronegative, negative ionic, hydrophobic, positive ionic and other) are represented by color codes. The occlusion maps symbolize the regions of favorable and unfavorable interactions.

Visually, Fig. 6A analysis illustrates the presence of the blue color cubes at the C3, C4, C5 positions of the phenyl ring, attached to the N-2 of hydroxamate core and was pointing toward the positive potential of electron withdrawing attribute of the molecules and was necessary for the activity at this particular position. It was also suggestive of the fact that the addition of suitable electron withdrawing groups at the C3, C4, C5 positions of the phenyl ring sites will add on the MMP-9 inhibition activity, whereas the addition of electron withdrawing groups near C2 and C6 position of the phenyl ring will contribute to decreased receptor binding, which in turn will result in lower potency of compounds.

Fig. 6B demonstrates the volume occlusion map for other feature. The map showed the presence of only blue color region at the C2/3, C3/4 and C4/5 positions of the phenyl ring favor the MMP-9 inhibitory activity; however the less dense occlusion map shows the little influence of this variable on the MMP-9 activity.

The volume occlusion maps of negative ionic feature (Fig. 6C) illustrate the spatial arrangement of favorable ionic interactions to the acceptor groups at the C3 and C4 positions of the phenyl ring. The occlusion map analysis depicts that blue cubes at the meta and para positions of the phenyl ring explain a favorable ionic group to an acceptor group available in the protein.

The volume occlusion maps of positive ionic feature (Fig. 6D) describe the favorable ionic interactions to donor groups at the C4 position of the phenyl ring.

Fig. 6E illustrates the effect of hydrophobic groups on MMP-9 inhibitory activity. Inference can be drawn from the picture that hydrophobic groups (blue cubes) were well tolerated near C2/3, C3/4 positions of the phenyl ring on hydroxamate moiety, whereas the substitution of hydrophobic groups at C1/2, C4/5, C5/6 of the phenyl ring site were intolerable (red cubes) or may hamper the binding of the molecules to the active site receptor which results in decreased MMP-9 inhibition.

Overall, the all atom QSAR model generated by PHASE depicts that substitution at C3, C4 and C5 by different groups like electron-withdrawing, ionic and/or hydrophobic groups play an important role in the MMP-9 activity. The substitutions at other positions i.e. C2 and C6 were not having any significant contribution in the biological activity.

Conclusion

In the current research work, pharmacophore and 3D-QSAR models using an all atom based approach implied in PHASE module of Schrodinger Modeling Suite were generated for the prediction of MMP-2 and MMP-9 inhibitory activities of the hydroxamate derivatives, a series of potent MMP-2 and MMP-9 inhibitors. Best pharmacophore hypothesis with AAARR features having a site score 0.91, vector score 0.991, and volume score 0.842 was selected to be the common pharmacophore hypothesis and was used further for the development of 3D-QSAR models. The all atom based 3D-QSAR models resulted in valid statistical results and showed good internal and external consistencies. The selected models were greatly significant as revealed by the correlation and predictive statistics to sketch unambiguous inferences. The resulting 3D-QSAR models were further derived to identify the three-dimensional arrangements of various substituents affecting the MMP inhibition, using the volume occlusion colored maps. The generated maps explained how and up to what extent hydrophobic, electron withdrawing and H-donor groups in the molecular structure influenced the MMP-2 and MMP-9 inhibitory potential showed by the dataset compounds. The generated volume occluded maps demonstrated that the MMP-2 and MMP-9 inhibitory activity can be increased, if the electron-withdrawing feature near phenyl ring of hydroxamate was supplemented by suitable functional groups and by the assimilation of H-donor, hydrophobic, and positive ionic groups at particular positions in the molecules. In addition, the results also confirmed the closed connection of the 5 point AAARR pharmacophore hypothesis which was used for 3D-QSAR models and to that of the binding mode of hydroxamates and the validation of the pharmacophore hypothesis was done. Overall, the developed QSAR models may be used for biological activity prediction and rational design of potential MMP-2 and MMP-9 inhibitors.

List of abbreviations

3D-QSAR	3-dimensional quantitative structure–activity relationship
MMP	matrix metalloproteinase
MT1-MMP	membrane type matrix metalloproteinase
PLS	partial least square
LFER	linear free energy related
CoMFA	comparative molecular field analysis
CoMSIA	comparative molecular similarity indices analysis
RMSD	relative mean square deviation
RMSE	root-mean-square error
SD	standard deviation
r^2	correlation coefficient

Authors' contributions

Viney Lather (VL) proposed the subject, designed methods and experiments of the study and supervised the entire work. Harish Dureja (HD) was involved in the commencement of the proposal, revised the manuscript decisively and had provided final version approval to be published. Dharmender Rathee (DR) performed the in silico experimental work, done data analysis and interpretation of results and prepared the draft of the manuscript. VL modified the manuscript. All the authors read and approved the final manuscript.

Conflicts of interest

The authors declare no conflicts of interest.

Acknowledgements

We wish to thank the Dept. of Pharmaceutical Sciences, M.D. University, Rohtak and the management of JCDM College of Pharmacy for providing the facilities and uninterrupted support to carry out the work.

References

Combs, A. P. (2007). Structure-based drug design of new leads for phosphatase research. *Investigational Drugs*, *10*(2), 112–115.

Coumar, M. S., Leou, J. S., Shukla, P., Wu, J. S., Dixit, A. K., Lin, W. H., et al. (2009). Structure-based drug design of novel Aurora kinase A inhibitors: Structural basis for potency and specificity. *Journal of Medicinal Chemistry*, *52*, 1050–1062.

Dixon, S. L., Smondyrev, A. M., Knoll, E. H., Rao, S. N., Shaw, D. E., & Friesner, R. A. (2006). PHASE: A new engine for pharmacophore perception, 3D QSAR model development, and 3D database screening: 1. Methodology and preliminary results. *Journal of Computer Aided Molecular Design*, *20*, 647–671.

Dureja, H., Kumar, V., Gupta, S., & Madan, A. K. (2007). Topochemical models for the prediction of lipophilicity of 1,3-disubstituted propan-2-one analogs. *Journal of Theoretical and Computational Chemistry*, *6*, 435–448.

Egeblad, M., & Werb, Z. (2002). New functions for the matrix metalloproteinases in cancer progression. *Nature Reviews Cancer*, *2*, 161–174.

Folkman, J. (1971). Tumor angiogenesis: Therapeutic implications. *New England Journal of Medicine*, *285*, 1182–1186.

Guner, O. F. (2000). *Pharmacophore perception, development and use in drug design*. San Diego, CA, USA: International University Line.

Gupta, S. P. (2015). QSAR studies on hydroxamic acids: A fascinating family of chemicals with a wide spectrum of activities. *Chemical Reviews*, *115*, 6427–6490.

Johnson, L. L., Dyer, R., & Hupe, D. J. (1998). Matrix metalloproteinases. *Current Opinion in Chemical Biology*, *2*, 466–471.

Katritzky, A. R., Mu, L., Lobanov, V. S., & Karelson, M. (1996). Correlation of boiling points with molecular structure. 1. A training set of 298 diverse organics and a test set of 9 simple inorganics. *Journal of Physical Chemistry*, *100*, 10400–10407.

Khan, A., Prakash, A., Kumar, D., Rawat, A., Srivastava, R., & Srivastava, R. (2010). Virtual screening and pharmacophore studies for ftase inhibitors using Indian plant anticancer compounds database. *Bioinformation*, *5*, 62–66.

Kontogiorgis, C. A., Papaioannou, P., & Hadjipavlou-Litina, D. J. (2005). Matrix metalloproteinase inhibitors: A review on pharmacophore mapping and (Q)SARs results. *Current Medicinal Chemistry*, *12*, 339–355.

Lather, V., Kristam, R., Singh, J. S., Kristam, R., Karthikeyan, N. A., & Balaji, V. N. (2008). QSAR models for prediction of glycogen synthase kinase-3b inhibitory activity of indirubin derivatives. *QSAR Combinatorial Science*, *27*(6), 718–728.

Li, J., Zhang, Y. P., & Kirsner, R. S. (2003). Angiogenesis in wound repair: Angiogenic growth factors and the extracellular matrix. *Microscopy Research & Technique*, *60*, 107–114.

Liekens, S., Clercq, E. D., & Neyts, J. (2001). Angiogenesis: Regulators and clinical applications. *Biochemical Pharmacology*, *61*, 253–270.

Mori, M., Massaro, A., Calderone, V., Fragai, M., Luchinat, C., & Mordini, A. (2013). Discovery of a new class of potent MMP inhibitors by structure based optimization of the arylsulfonamide scaffold. *ACS Medicinal Chemistry Letters*, *4*, 565–569.

Morphy, J. R., Millican, T. A., & Porter, J. R. (1995). Matrix metalloproteinase inhibitors: Current status. *Current Medicinal Chemistry*, *2*, 743–762.

Mustata, G., Li, M., Zevola, N., Bakan, A., Zhang, L., Epperly, M., et al. (2011). Development of small-molecule PUMA inhibitors for mitigating radiation-induced cell death. *Current Topics in Medicinal Chemistry*, *11*, 281–290.

Nirmala, G., Adimulam, Y. B., & Seetharamaiah, P. (2016). In P. V. Lakshmi, P. V. Lakshmi, et al. (Eds.), *Computational intelligence techniques in health care. Springer briefs in forensic and medical bioinformatics*.

Phase. (2008). *Version 3.0*. New York, NY: Schrodinger LLC.

Rathee, D., Thanki, M., Bhuva, S., Anandjiwala, S., & Agrawal, R. (2013). Iridoid glycosides-Kutkin, Picroside I, and Kutkoside from *Picrorrhiza kurroa* Benth inhibits the invasion and migration of MCF-7 breast cancer cells through the down regulation of matrix metalloproteinases. *Arabian Journal of Chemistry*, *6*, 49–58.

Roy, K., Pal, D. K., De, A. U., & Sengupta, C. (2001). QSAR of matrix metalloproteinase inhibitor N-[(substituted phenyl)sulfonyl]-N-4-nitrobenzylglycine hydroxamates using LFER model. *Drug Design and Discovery*, *17*(4), 315–323.

Scozzafava, A., & Supuran, C. T. (2000). Protease inhibitors: Synthesis of potent bacterial collagenase and matrix metalloproteinase inhibitors incorporating *N*-4-nitrobenzylsulfonylglycine hydroxamate moieties. *Journal of Medicinal Chemistry*, *43*, 1858–1865.

Skiles, J. W., Gonnella, N. C., & Jeng, A. Y. (2001). The design, structure, and therapeutic application of matrix metalloproteinase inhibitors. *Current Medicinal Chemistry*, *8*, 425–474.

Stephen, H., Nicolas, M., Cécile, G., & Martin, V. (2001). N-aryl sulfonyl homocysteine hydroxamate inhibitors of matrix metalloproteinases: Further probing of the S1, S1, and S2 pockets. *Journal of Medicinal Chemistry*, *44*, 3066–3073.

Stetler-Stevenson, W. G. (1999). Matrix metalloproteinases in angiogenesis: A moving target for therapeutic intervention. *Journal of Clinical Investigation*, *103*, 1237–1241.

Subramaniam, R., Malik, S., & Srivastava, D. K. (2009). Natural products as inhibitors of matrix metalloproteinases. In *Natural products: Chemistry, biochemistry and pharmacology*. pp. 54–79. Narosa Publishing House.

Summers, J. B., & Davidsen, S. K. (1998). Matrix metalloproteinase inhibitors and cancer. *Annual Reports in Medicinal Chemistry*, *33*, 131–140.

van Montfort, R. L., & Workman, P. (2009). Structure-based design of molecular cancer therapeutics. *Trends in Biotechnology*, *27*, 315–328.

Vihinen, P., & Kähäri, V. M. (2002). Matrix metalloproteinases in cancer: Prognostic markers and therapeutic targets. *International Journal of Cancer*, *99*, 157–166.

Weinstat-Saslow, D., & Steeg, P. S. (1994). Angiogenesis and colonization in the tumor metastatic process: Basic and applied advances. *FASEB Journal*, *8*, 401–407.

Wilson, G. M., & Muftuoglu, Y. (2012). Computational strategies in cancer drug discovery. *Advances in Cancer Management*, 237–254.

Wold, S. (1991). Validation of QSAR's. *Quantitative Structure-Activity Relationships*, *10*, 191–193.

Yu, Q., & Stamenkovic, I. (2000). Cell surface-localized matrix metalloproteinase-9 proteolytically activates TGF-β and promotes tumor invasion and angiogenesis. *Genes & Development*, *14*, 163–176.

Zask, A., Levin, J. I., Killar, L. M., & Skotnicki, J. S. (1996). Inhibition of matrix metalloproteinases: Structure based design. *Current Pharmaceutical Design*, *2*, 624–661.

Zheng, J., Wen, R., & Guillaume, D. (2008). Three-dimensional quantitative structure–activity relationship (CoMFA and CoMSIA) studies on galardin derivatives as gelatinase A (matrix metalloproteinase 2) inhibitors. *Journal of Enzyme Inhibition and Medicinal Chemistry*, *23*(4), 445–453.